



HAL
open science

On Mn²⁺ EPR Probing of the Ferroelectric Transition and Absence of Magnetoelectric Coupling in Dimethylammonium Manganese Formate (CH₃)₂NH₂Mn(HCOO)₃, a Metal–Organic Complex with the Pb-Free Perovskite Framework

Nandita Abhyankar, Sylvain Bertaina, Naresh S. Dalal

► **To cite this version:**

Nandita Abhyankar, Sylvain Bertaina, Naresh S. Dalal. On Mn²⁺ EPR Probing of the Ferroelectric Transition and Absence of Magnetoelectric Coupling in Dimethylammonium Manganese Formate (CH₃)₂NH₂Mn(HCOO)₃, a Metal–Organic Complex with the Pb-Free Perovskite Framework. *Journal of Physical Chemistry C*, 2015, 119 (50), pp.28143 - 28147. 10.1021/acs.jpcc.5b10326 . hal-01699844

HAL Id: hal-01699844

<https://amu.hal.science/hal-01699844>

Submitted on 2 Feb 2018

HAL is a multi-disciplinary open access archive for the deposit and dissemination of scientific research documents, whether they are published or not. The documents may come from teaching and research institutions in France or abroad, or from public or private research centers.

L'archive ouverte pluridisciplinaire **HAL**, est destinée au dépôt et à la diffusion de documents scientifiques de niveau recherche, publiés ou non, émanant des établissements d'enseignement et de recherche français ou étrangers, des laboratoires publics ou privés.

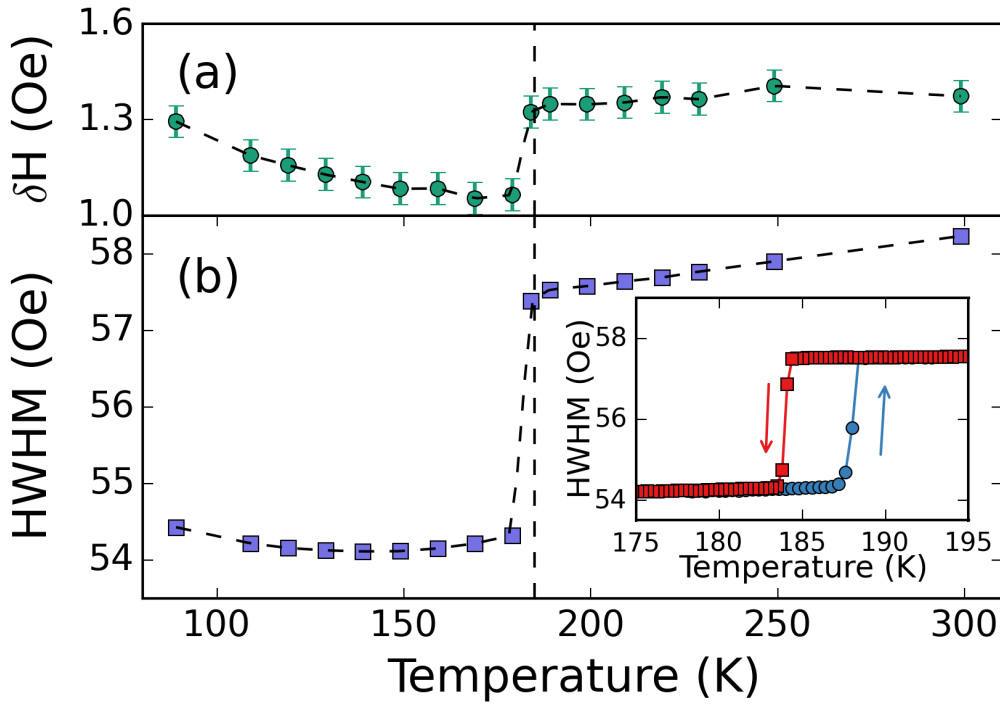
**On Mn²⁺ EPR Probing of the Ferroelectric
Transition and Absence of Magnetoelectric
Coupling in Dimethylammonium Manganese
Formate (CH₃)₂NH₂Mn(HCOO)₃ , a Metal-
Organic Complex with the Pb-Free Perovskite
Framework**

N. Abhyankar[#], S. Bertaini^{†}, N. S. Dalal^{*†}*

[#] Department of Chemistry and Biochemistry, Florida State University, Tallahassee, FL, 32306-4390, USA

[†] Aix-Marseille Université, CNRS, IM2NP UMR7334, 13397 cedex 20, Marseille, France

ABSTRACT : We employ electron paramagnetic resonance (EPR) of Mn^{2+} as a spin probe to study the paraelectric–ferroelectric transition in Dimethylammonium Manganese Formate, $[(CH_3)_2NH_2]Mn(CHCO_2)_3$, (DMMnF), which is considered a model metal-organic framework (MOF) with a Pb-free perovskite architecture. We study the variation of the Mn^{2+} EPR line shape and intensity at the X-band (~ 9.5 GHz) over 80K to 300 K. The peaks are essentially Lorentzian, implying electron spin exchange at frequencies greater than 9.5 GHz. On cooling, an anomalous increase in the peak width is noted at 185 K but no anomalous change in the normalized, double-integrated EPR signal intensity around the T_c , indicating that DMMnF is transparent to microwave electric fields with a clear lack of magnetoelectric coupling, in contrast to an earlier report. Our analysis enables us to estimate change in lattice strain related to the ferroelectric transition, information that is difficult to obtain by other techniques.



1. INTRODUCTION

Inorganic perovskites with the formula ABO_3 , where A is a divalent cation such as Pb or Bi, and B a transition ion (e.g., Mn), have received increased research focus recently, in part because they offer new possibilities in nanotechnology , with potential applications in information storage and manipulation via both electric and magnetic pulses on a single-phase material.¹⁻⁴ Such materials which display simultaneous existence of more than one type of long-range order are termed multiferroics. Multiferroics exhibiting simultaneous magnetic and electric ordering offer the possibility of magnetoelectric coupling, which is the electric control of magnetization or magnetic control of dielectric polarization.^{1,2} However, reports of magnetoelectric coupling are rare even for single-phase inorganic materials, which have been extensively researched for several decades.

Based on eventual environmental concerns, it has been thought desirable to develop analogous materials but free of Pb,¹ and recently a class of Pb-free materials with the perovskite architecture and coexisting ferroelectric – ferromagnetic characteristics has been reported.⁵⁻¹² The forerunner of this class is the compound Dimethylammonium Zinc Formate, $[(CH_3)_2NH_2]Zn(HCOO)_3$, which becomes ferroelectric at 156 K ⁵ and which exhibits glassy behavior akin to the inorganic perovskites, ⁶ The Mn analogue of this compound, Dimethylammonium Manganese Formate, $[(CH_3)_2NH_2]Mn (HCOO)_3$, turns ferroelectric below 185 K , and becomes a canted antiferromagnet at 8.5 K ⁷ .

The compound $[(CH_3)_2NH_2][Mn (HCOO)_3]$, henceforth referred to as DMMnF , is the first reported metal-organic multiferroic (MOF) with the perovskite architecture. It is a Type II multiferroic in which magnetic and electric order have different origins. It undergoes a transition from a paraelectric to ferroelectric state when cooled to ~ 185 K. This transition results from the ordering

of hydrogen bonds between the DMA⁺ protons and formate-group oxygens (Figure 1). In the paraelectric state, the nitrogen in DMA⁺ undergoes hindered rotation and is disordered over three possible positions. At the phase transition, T_c, the hindered rotation slows down drastically and the DMA⁺ ion gets ordered into one of the three positions, accompanied by a structural phase transition.^{5,13,14} Polarization develops as a result of the structural distortion of the DMA⁺ cation due to the hydrogen bonding, although the exact mechanism of this transition is still not fully elucidated. On the other hand, the MOF undergoes a magnetic phase transition to a canted antiferromagnetic state due to the Mn²⁺ ions at ~8.5 K. The large separation of electric and magnetic phase transitions and the split-order nature of magnetic and electric order makes it unlikely that there is magnetoelectric coupling in DMMnF¹⁵. This is consistent with the absence of reports on electric control of magnetization or vice versa in this MOF. Nonetheless, perovskite-like MOFs with paramagnetic metal ions are currently the most extensively explored systems with the view of obtaining magnetoelectric coupling in hybrid, single-phase multiferroic materials.¹⁷

With this in view, recently Wang et al.¹⁶ have carried out detailed magnetic susceptibility, magnetization, dielectric polarization and electron paramagnetic resonance (EPR) on DMAMnF. In particular, they have used the EPR of the naturally present Mn²⁺ ion as a spin probe of the ferroelectric transition at T_c ~ 185 K, since EPR can indeed provide detailed information on the local symmetry and molecular dynamics at the site of a spin probe.^{17,18} These authors conclude that the temperature variation of intensity of the EPR peak and of the magnetic susceptibility provided a direct evidence of the existence of a strong magnetoelectric coupling in DMAMnF, and thus an easy, new methodology for measuring magnetoelectric couplings in new multiferroic samples, in contrast to an earlier EPR and magnetization report on DMAMnF⁶. This issue

provided an incentive for the present undertaking, in which we have carried out detailed EPR measurements on single crystals and powders of DMAMnF, using two different types of microwave cavities to obviate any possible errors associated with the change in the cavity quality (Q) factor at a ferroelectric transition^{19,20} as a result of the possible dielectric loss at the ferroelectric transition. The presently reported EPR measurements, involving an internal spin standard, do not show any signature in the drop in EPR intensity at the ferroelectric transition. Magnetic susceptibility measurements at microwave frequency or DC SQUID data also did not detect any significant deviation from the Curie behavior around the T_c . The structural transition observed by the EPR linewidth has no effect on the susceptibility which leads us to the conclusion that there is little to no magnetoelastic effect in DMAMnF in agreement with Thomson et al.²¹ A likely cause of discrepancy is discussed.

2. EXPERIMENTAL DETAILS:

Synthesis: Dimethylammonium manganese formate, DMMnF, was synthesized using a standard solvothermal synthetic procedure, described in previous reports.^{5,6} Briefly, 1 mmol of $MnCl_2 \cdot 4H_2O$ was dissolved in a solution consisting of 6 mL Dimethylformamide and 6 mL deionized water. The solution was heated in a Teflon-lined autoclave at 140°C for three days. The supernatant was decanted and left to crystallize, yielding clear, block single crystals after several days. Crystals of Mn²⁺-doped Dimethylammonium Zinc Formate, DMZnF-Mn, were synthesized by the same method with Zn: Mn mole ratios in the initial reaction mixture being 1: 400.

Single Crystal X-Ray Diffraction: The structural identity was verified by single crystal x-ray diffraction, using a BRUKER SMART APEX II diffractometer, equipped with a graphite monochromator and Mo $K\alpha$ ($\lambda = 0.71073 \text{ \AA}$) radiation source. Measurements were made at 200

K and 100 K respectively, with a sample cooling rate of 2 K/min. The deduced space group, and the derived bond lengths and bond angles agreed fully with earlier reports.^{13,14} DMAMnF unit cell structure is shown in Figure 1.

SQUID: SQUID measurements were carried out on powdered samples of DMMnF, using a Quantum Design MPMS. Temperature sweeps were carried out in the range of 1.8-300 K under an applied field of 100 G.

EPR: EPR experiments have been performed using a conventional X-band Bruker EMX spectrometer operating at about 9.4 GHz between 80 K and 300 K. The temperature was controlled by an Oxford ITC and stabilized 10min between each spectrum. Near the ferroelectric transition (about $T_c=185$ K) a thermal ramp of 0.5 K/min was applied and EPR spectra was recorded continuously. Temperature steps of 0.25 K and even 0.1 k were utilized around T_c . Closer temperature A small amount of DPPH was used as reference in order to avoid intensity artifacts du to variation of the Q factor of the cavity. Magnetic field modulation associated with a lock-in detection was employed resulting in derivative of the signal. All measurements have been carried out for the static field H perpendicular to the (012) face of the crystal. All the spectra recorded can be fitted by a derivative of a Lorentzian. The simultaneous fit of the DMMnF signal and DPPH signal yield intensity, linewidth and resonance field with high accuracy and ensure removal of unwanted effects caused by the cavity.

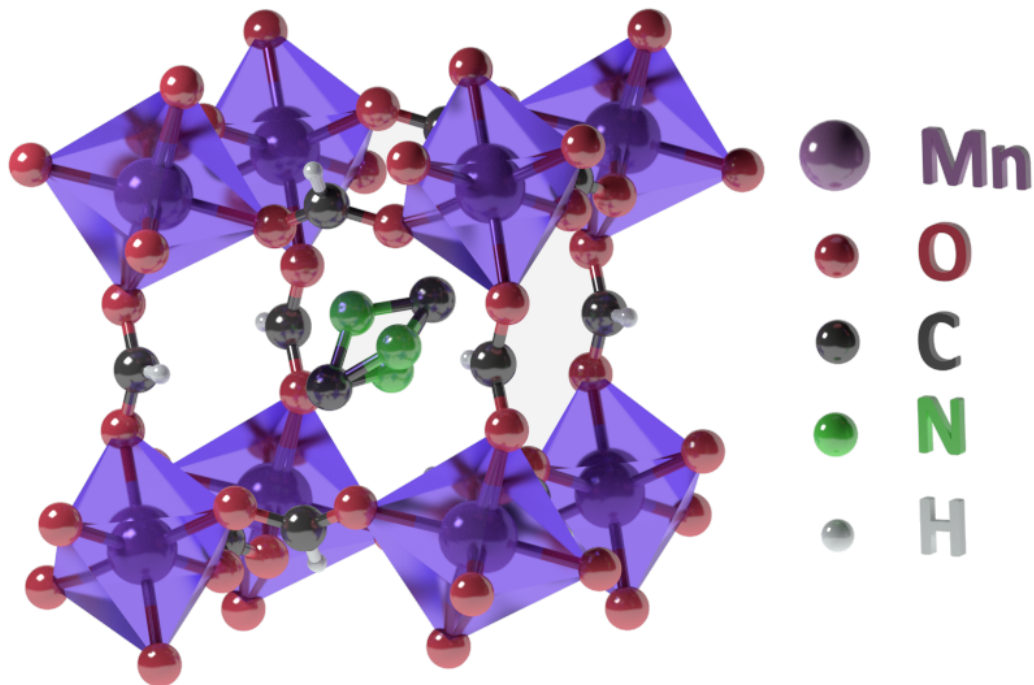


Figure 1: ABX₃-type MOF cavity in the paraelectric phase ($T > T_c$) of DMMnF. Mn²⁺ and HCOO⁻ ions form the porous framework. The cavity is occupied by the DMA⁺ ion. The Nitrogen in DMA⁺ is disordered over three positions at $T > T_c$ but gets ordered in one of the three positions below T_c .

3. RESULTS AND DISCUSSION:

EPR resonance field and linewidth: Temperature dependence of the continuous wave (cw) EPR of DMMnF has been carried out in the range 300 K down to 80 K with particular attention near the structural phase transition ($T_c \sim 185$ K). Figure 2 shows a series of spectra near T_c , in 10 K intervals from $T = 210$ K to $T = 160$ K. The sharp peak is the DPPH reference and the broader line is attributed to DMAMnF. There is a small but clear jump in DMMnF signal height when T_c is crossed.

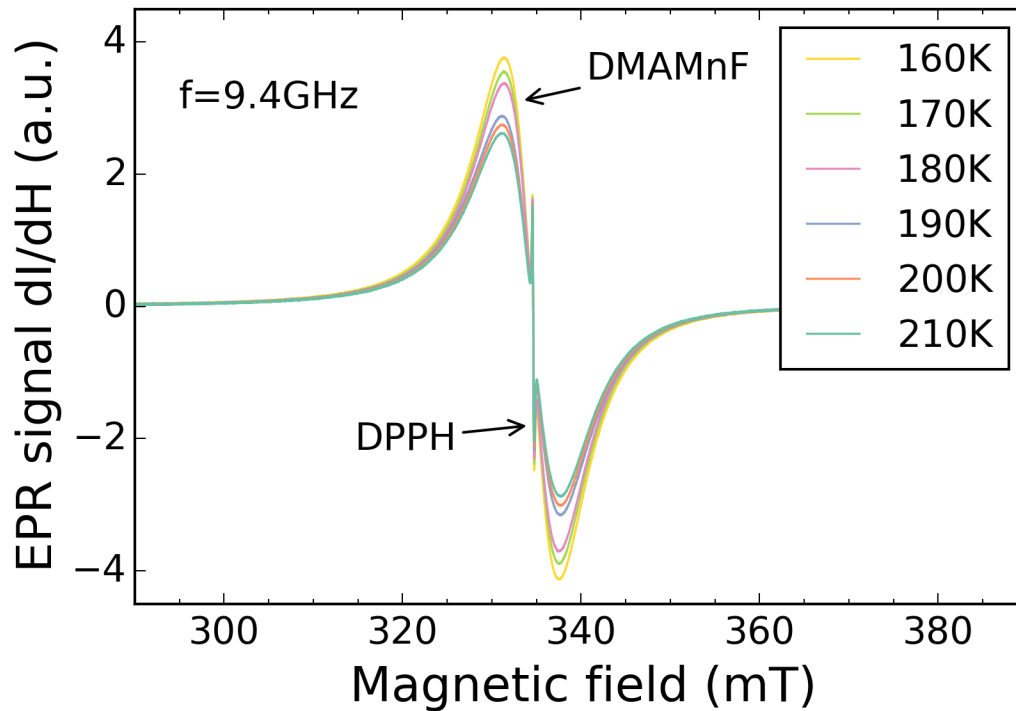


Figure 2: Comparison of X-band spectra on DMAMnF single crystal in a range of temperatures above and below T_c (~ 185 K). The sharp small line in the middle is due to the internal standard DPPH. As such, while this observation is in accord with those of Wang et al.⁶, additional studies after double integration showed no jump in the overall signal intensity (see below).

The EPR spectra were fitted using a derivative of a Lorentzian. The linewidth, resonance field and normalized intensity were extracted from fits. Figure 3 (a) shows the temperature dependence of shift of the resonance field (δH) compared to the resonance field of DPPH (which is temperature-independent). DMAMnF is highly isotropic and its g-factor is very close to the free-electron value. However one can see a small but clear variation of δH when temperature crosses T_c . Figure 3 (b) shows the temperature dependence of the half width at half maximum (HWHM). The HWHM is broadly constant with temperature but there is a clear discontinuity in HWHM when temperature crosses T_c . In order to observe the effect of the phase transition on the

linewidth, we used a slow thermal ramp and recorded spectra at closely spaced intervals of 0.5 K. The inset in Figure 3 shows the HWHM while cooling (red squares) and heating (blue circles). Not only is the variation of HWHM almost instantaneous but a clear hysteresis of 5K is reported. The presence of the hysteresis is evidence of an irreversible process caused by a first order structural phase transition.

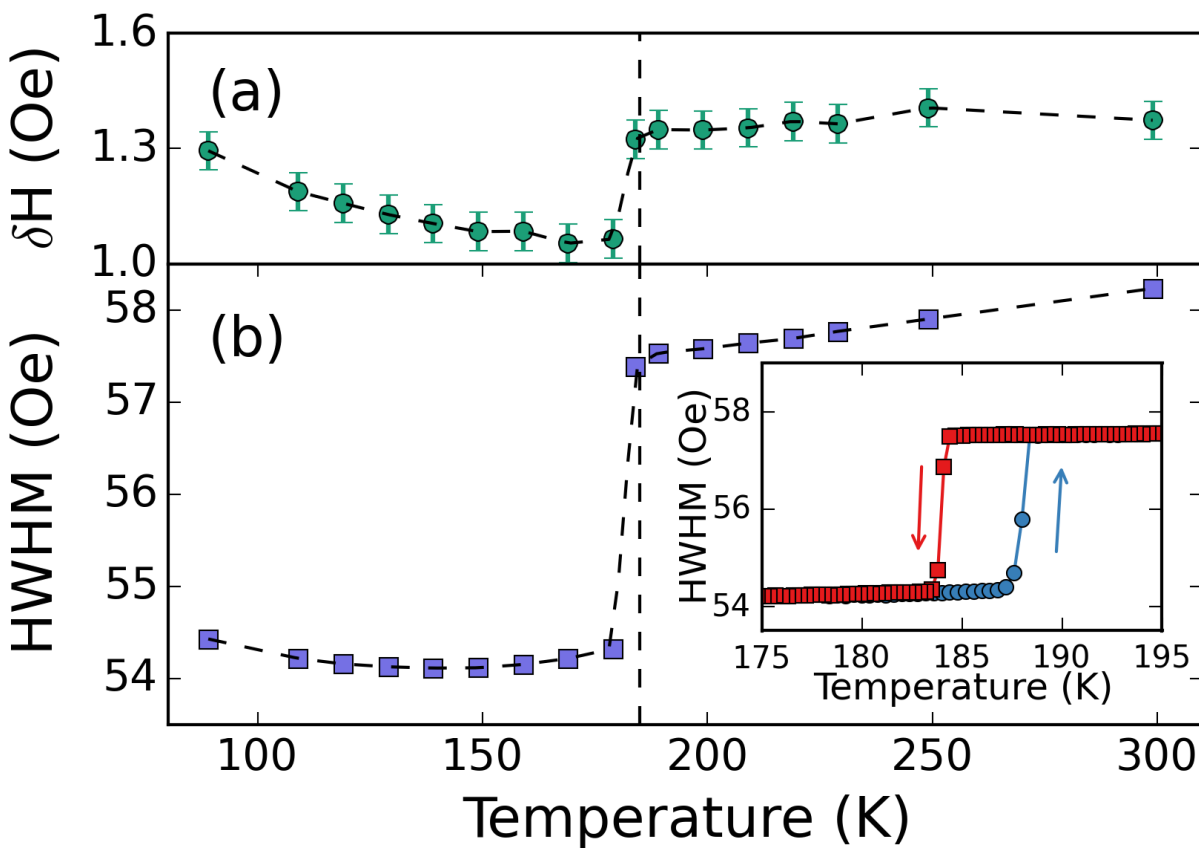


Figure 3: Comparison of temperature-dependences of (a) resonance field and (b) linewidth of the X-band EPR signal from a DMMnF single crystal. The inset in (b) shows the change in linewidth at 0.5 K intervals around the phase transition.

In the following, we will show that the HWHM value and variation can be explained by a standard Anderson-Weiss (AW) ²² analysis taking into account the motion of DMA⁺ cation. In the AW model, the atom absorbs a single frequency which varies over a distribution of the local fields but also varies randomly in time by the exchange interaction: the exchange narrowing model. The electron spins feel a local field modified by many interactions like dipole-dipole interactions, (super)hyperfine interactions, and local modulations of the crystal field. These interactions are responsible of a broadening of the EPR lines. On the other hand the electron spins also feel a time fluctuating field due to the Heisenberg exchange interaction which results in line narrowing. Usually the local field distribution is due to dipole-dipole interactions. The linewidth due to the combination of line broadening and narrowing mechanisms can be estimated by Equation 1 below.

$$\Delta H = \frac{H_p^2}{H_e} \quad \text{-- (1)}$$

with $H_p^2 = 5.1(g\beta n)^2 S(S+1)$, is the dipolar second moment and $H_e = 1.68 \frac{J}{g\beta} \sqrt{S(S+1)}$ is the exchange field. $S = 5/2$ and β is the Bohr magneton. To describe DMAMnF we choose $J=0.32\text{cm}^{-1}$, $n = \text{number density} = 4.4 \cdot 10^{21}$ spins/cm³ (calculated using unit cell parameters for the high temperature, R3c phase) and $g=2$. We obtain $H_p^2 = 291000 \text{ Oe}^2$ ($H_p=539.4 \text{ G}$) and $H_e=16900 \text{ G}$. Since H_e is higher than the resonance field (about 3300Oe) the “10/3 effect” takes place and the HWHM is: $\Delta H=10/3 \cdot 16.7\text{G} = 55 \text{ G}$.

This value is in agreement with the HWHM observed in Figure 3b. However, the sudden change of HWHM at T_c cannot be explained only by the change in dipolar broadening due to structural phase transition. Indeed, the variation of number of spins per unit volume, n is negligible

between the 2 structural phases and other parameters in equation (1) also do not change at the phase transition. We can explain this jump in HWHM by the motion of the DMA⁺ cation. At high temperature, the DMA⁺ moves in the cage between its 3 equivalent positions. This motion locally changes the crystal field around the Mn²⁺ ions and acts like D-strain. For T < T_c, the DMA⁺ stops moving and the crystal field doesn't fluctuate anymore. This effect is usually observed in ferroelastic phase transitions ²⁴ investigated by EPR of transition metal impurities (mostly Mn²⁺). To estimate broadening induced due to motion of DMA⁺ we performed EPR on the non-magnetic but equivalent system Dimethylammonium Zinc Formate (DMZnF) lightly doped with Mn²⁺ (< 0.5%). Like DMMnF, DMZnF exhibits a paraelectric /ferroelectric transition associated with a structural change (see Figure 1 in Supporting Information). In Mn²⁺-doped DMZnF, the Mn²⁺ ions are too far from each other and have a negligible dipole-dipole as well as exchange interaction. Only broadening due to crystal field strain is observed. From simulations of the EPR spectra we extract the strain field H_{st} seen by the Mn²⁺ ions. At high temperature H_{st}^{ht} ~ 150 Oe and at low temperature H_{st}^{lt} ~ 10 Oe. The extended AW model can be shown by Equation 2 below.

$$\Delta H = \frac{10}{3} \frac{H_p^2 + H_{st}^2}{H_e} \quad \text{-- (2)}$$

It is important to notice the H-strain broadening or H_{st} is reduced by the time fluctuation caused by the exchange field. The HWHM now becomes:

$$\Delta H^{\text{ht}} = \frac{10}{3} * \frac{291000 + 150^2}{16900} = 62\text{G}$$

$$\Delta H^{\text{lt}} = \frac{10}{3} * \frac{291000 + 10^2}{16900} = 57\text{G}$$

These values are consistent with the ones reported in Figure 3, supporting our argument that the mechanism of the observed width is reasonably well understood. Our analysis of EPR lineshape enables us to probe the evolution of structural strain through the ferroelectric phase transition.

This information is difficult to obtain by other techniques.

The same arguments can be applied to shift in resonance field δH shown in Figure 3a since it's a local effect only affected by the crystal field. It is interesting to notice that the ferroelastic phase transition is rarely observed in correlated magnets since its effect is highly reduced by the exchange narrowing effect. Finally it is seen the anomalies in δH and HWHM can be attributed to the structural phase transition, without invoking any magnetoelectric effect.

Magnetic susceptibility

To check for change in magnetic behavior at the ferroelectric phase transition, we carried out detailed SQUID measurements in the region of the ferroelectric phase transition. Susceptibility is given by the intensity of the EPR signal and extracted by the fits. Since intensity is highly dependent on the Q factor of the spectrometer cavity which itself can change with the temperature and during the ferroelectric transition, we used the DPPH signal as a reference for susceptibility. The DC susceptibility measurements show Curie-Weiss behavior in the region from 300 K – 30 K with $\theta = -13\text{K}$, as shown by the linearity of the $1/\chi_{\text{dc}}$ plots in this temperature range (Figure 4). This result is in agreement with previously published results “but in disagreement with Wang et al.”. To resolve this discrepancy, we compared χ_{dc} with the susceptibility from EPR measurements. Using the Kramers-Kronig relation, the susceptibilities from EPR and from SQUID should be proportional. In figure 4 we can see $1/\chi_{\text{ESR}}$ is perfectly linear in temperature with $\theta_{\text{ESR}} = -20\text{K}$ and no sign of ferroelectric transition is observed. The ferroelastic transition observed by the EPR

linewidth has no effect on the susceptibility which leads us to the conclusion that there is little to no magnetoelastic effect in DMMnF in agreement with Thomson et al.²¹ Additionally, we found that the deviation in linearity in the temperature dependence of χ^{-1} reported by Wang et al may be explained by the presence of a ferromagnetic impurity. When such a contribution is accounted for, the plot becomes linear as shown in the inset in Figure 4. Finally, the absence of any effect of the para/ferroelectric phase transition on the magnetic susceptibility proves there is no magnetoelectric coupling in paramagnetic phase in DMMnF.

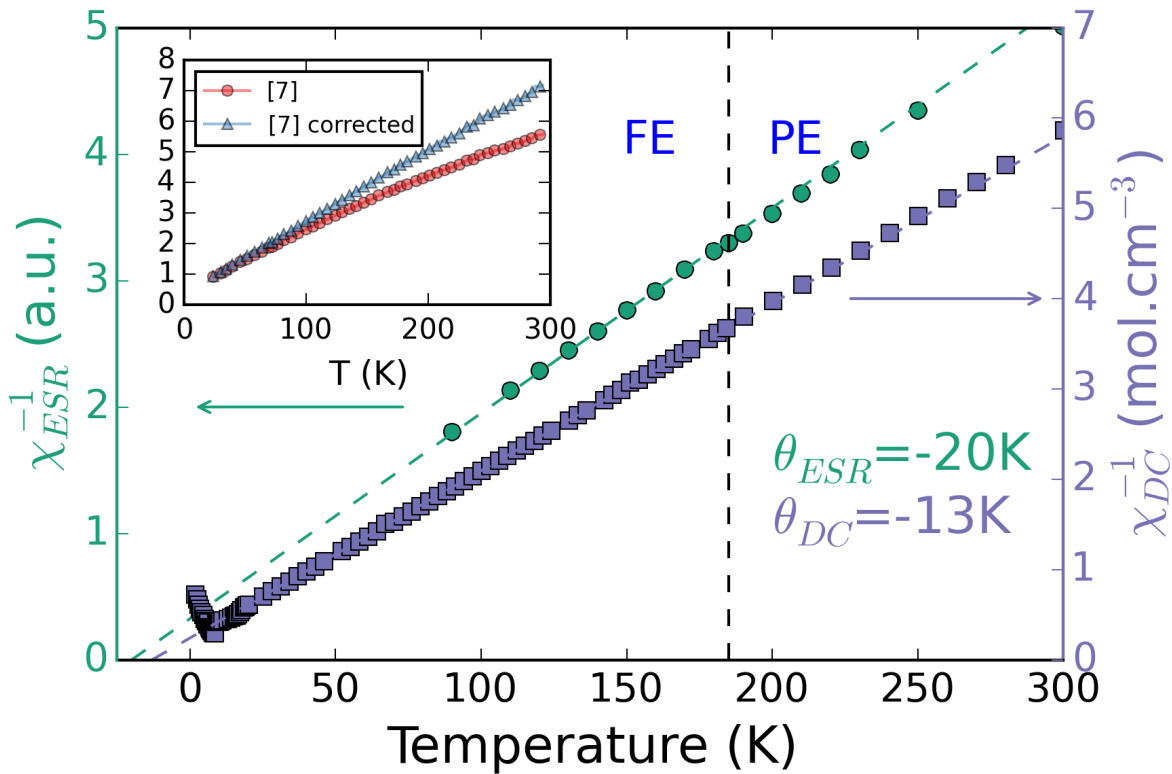


Figure 4: Comparison of temperature dependence of inverse susceptibility obtained from DC SQUID measurements (purple squares) and EPR (green circles). The inset shows inverse susceptibility as reported by Wang et al.,²⁶ and inverse susceptibility from Wang et al after correction for ferromagnetic contribution.

CONCLUSION:

We used EPR and SQUID magnetometry in order to probe the effect of the ferroelectric phase transition on the magnetic properties of DMMnF . Using the Anderson-Weiss model we described the anomaly observed at T_c by a structural phase transition. The movement of the DMA^+ cation in the high temperature phase results in a distribution of local crystal fields around the Mn^{2+} ions. When $T < T_c$ the DMA^+ ions order cooperatively and the distribution in local crystal fields is reduced. Magnetic susceptibility from EPR and from SQUID show a standard Curie-Weiss behavior and no sign of effect of the ferroelectric transition is observed, leading to the conclusion that neither a magnetoelastic coupling nor magnetoelectric coupling is observed in the paramagnetic phase of DMMnF . We also show that a recent report of magnetoelectric coupling can be explained by the presence of ferromagnetic impurities

ASSOCIATED CONTENT

Supporting Information. The Supporting Information provides the experimental and simulated spectra for DMZnF powder samples. This material is available free of charge via the Internet at <http://pubs.acs.org>

AUTHOR INFORMATION

Corresponding Authors

* Prof. Naresh Dalal, Department of Chemistry and Biochemistry, Florida State University, Tallahassee, FL, 32306-4390, USA (Email: dalal@chem.fsu.edu, Phone: +1-850-644-3398, Fax:)

* Dr. Sylvain Bertaina, Aix-Marseille Université, CNRS, IM2NP UMR7334, 13397 cedex 20, Marseille, France (Email: sylvain.bertaina@im2np.fr, Phone : Fax :)

Author Contributions

The manuscript was written through contributions of all authors. All authors have given approval to the final version of the manuscript.

ACKNOWLEDGEMENTS

We want to thank the interdisciplinary French EPR network RENARD (CNRS - FR3443).

REFERENCES

1. Cheetham, A.K.; Rao, C.N.R., “There’s Room in the Middle”, *Science*, **2007**, *318*, 58-59.
2. Fiebig, M., “Revival of the Magnetoelectric Effect”, *J. Phys. D: Appl. Phys.*, **2005**, *38*, R123-R152
3. Catalan, G.; Seidel, J.; Ramesh, R.; Scott, J.F., “Domain Wall Nanoelectrics”, *Rev. Mod. Phys.*, **2012**, *84*, 119-156.
4. Murray, L.; Dinca, M.; Long, J.R., “Hydrogen Storage in Metal-Organic Frameworks”, *Chem. Soc. Rev.*, **2009**, *38*, 1294-1314 .
5. Jain, P.; Dalal, N.S.; Toby, B.H.; Kroto, H.W.; Cheetham, A.K., “Order-Disorder Antiferroelectric Phase Transition in a Hybrid Inorganic-Organic Framework with the Perovskite Architecture”, *J. Am. Chem. Soc.*, **2008**, *130*, 10450-10451.
6. Besara, T.; Jain, P.; Dalal, N.S.; Kuhns, P.L.; Reyes, A.P.; Kroto, H.W.; Cheetham, A.K., “Mechanism of the Order-Disorder Transition, and Glassy Behavior in the Metal-Organic Framework $[(\text{CH}_3)_2\text{NH}_2]\text{Zn}(\text{HOO})_2$ ”, *Proc. Nat. Acad. Sci.* **2011**, *108*, 6828-6832.

7. Jain, P.; Ramachandran, V.; Clark, R.J.; Zhou, H.D.; Toby, B.H.; Dalal, N.S.; Kroto, H.W.; Cheetham, A.K., "Multiferroic Behavior Associated with an Order-Disorder Hydrogen-Bonding Transition in Metal-Organic Frameworks (MOFs) with the Perovskite ABX₃ Architecture", *J. Am. Chem. Soc.* **2009**, *131*, 13625-13627.
8. Hu, K.-L., Kurmoo, M., Wang, Z., Gao, S.; "Metal–Organic Perovskites: Synthesis, Structures, and Magnetic Properties of [C(NH₂)₃][MII(HCOO)₃](M= Mn, Fe, Co, Ni, Cu, and Zn; C(NH₂)₃= Guanidinium)", *Chem. Eur. J.*, **2009**, *15*, 12050-12064
9. Xu, G.-C., Ma, X.-M., Zhang, L., Wang, Z., Gao, S., "Disorder–Order Ferroelectric Transition in the Metal Formate Framework of [NH₄][Zn(HCOO)₃]", *J. Am. Chem. Soc.*, **2010**, *132* (28), 9588-9590
10. Maczka, M., Ciupa, A., Gagor, A., Sieradzki, A., Pikul, A., Macalik, B., Drozd, M., "Perovskite Metal Formate Framework of [NH₂-CH⁺-NH₂][Mn(HCOO)₃]: Phase Transition, Magnetic, Dielectric, and Phonon Properties", *Inorg. Chem.*, **2014**, *53*(10), 5260-5268
11. Maczka, M., Pietraszko, Macalik, L., Sieradzki, A., Trzmiel, J., Pikul, A., "Synthesis and Order–Disorder Transition in a Novel Metal Formate Framework of [(CH₃)₂NH₂][Na_{0.5}Fe_{0.5}(HCOO)₃]", *Dalton Trans.*, **2014**, *43*, 17075-17084
12. Du, Z.-Y., Zhao, Y.-P., He, C.-T., Wang, B.-Y., Xue, W., Zhou, H.-L., Bai, J., Huang, B., Zhang, W.-X., Chen, X.-M., "Structural Transition in the Perovskite-like Bimetallic Azido Coordination Polymers: (NMe₄)₂[B' · B''(N₃)₆] (B' = Cr³⁺, Fe³⁺; B'' = Na⁺, K⁺)", *Cryst. Growth Des.*, **2014**, *14* (8), 3903-3909
13. Sánchez-Andújar, M., Presedo, S., Yáñez-Vilar, S., Castro-García, S., Shamir, J. and Señaris-Rodríguez, M. A., " Characterization of the Order-Disorder Dielectric Transition in

- the Hybrid Organic-Inorganic Perovskite-Like Formate $\text{Mn}(\text{HCOO})_3[(\text{CH}_3)_2\text{NH}_2]$ ", *Inorg. Chem.*, **2010**, *49*, 1510-1516
14. Mączka, M., Gağor, A., Macalik, B., Pikul, A., Ptak, M. and Hanuza, J., "Order–Disorder Transition and Weak Ferromagnetism in the Perovskite Metal Formate Frameworks of $[(\text{CH}_3)_2\text{NH}_2][\text{M}(\text{HCOO})_3]$ and $[(\text{CH}_3)_2\text{ND}_2][\text{M}(\text{HCOO})_3]$ (M = Ni, Mn)", *Inorg. Chem.*, **2014**, *53*, 457-467
 15. Khomskii, D. I., "Multiferroics: Different Ways to Combine Magnetism and Ferroelectricity", *J. Mag. Mag. Mat.*, **2005**, *306*, 1-8
 16. Wang, W.; Yan, O-Q.; Cong, J.Z.; Wang, F.; Shen, S-P.; Zou, T.; Zhang, D.; Wang, S-G.; Han, X-F.; Sun, Y., "Magnetoelectric Coupling in the Paramagnetic State of a Metal-Organic Framework", *Scientific Reports*, **2013**, *3*, 2024-2029.
 17. Dalal, N.S., "Electron Paramagnetic Resonance and ENDOR Studies of Slow Dynamics and the Central Peak Phenomenon near Phase Transitions", *Advan Mag. Reson.*, **1982**, *10*, 119-218
 18. J.Y. Buzaré, J.J. Rousseau and J.C. Fayet, "La paire $\text{Gd}^{3+}-\text{O}^{2-}$ dans RbCaF_3 : Une Sonde Sensible pour L'étude par R.P.E. de la Transition Structurale a 193 K", *J. Physique Lett.*, **1977**, *38*, 445-448
 19. Cage, B., Cevc, P., Blinc, R., Brunel, L.-C., Dalal, N. S., "1-370 GHz EPR Linewidths for K_3CrO_8 : A Comprehensive Test for the Anderson-Weiss Model", *J. Magn. Res.*, **1998**, *135*, 178-184
 20. van Tol, J., Brunel, L.-C., Wylde, R. J., "A Quasioptical Transient Electron Spin Resonance Spectrometer Operating at 120 GHz and 240 GHz", *Rev. Sci. Inst.*, **2005**, *76*, 074101

21. Thomson, R. I., Jain, P., Cheetham, A. K., Carpenter, M. A., “Elastic Relaxation Behavior, Magnetoelastic Coupling, and Order-Disorder Processes in Multiferroic Metal-Organic Frameworks”, *Phys. Rev. B.*, **2012**, *86*, 214304
22. Anderson, P. W., “Exchange Narrowing in Paramagnetic Resonance”, *Rev. Mod. Phys.*, **1953**, *25*, 1
23. Wang, X.-Y., Gan, L., Zhang, S.-W., Gao, S., “Perovskite-like Metal Formates with Weak Ferromagnetism and as Precursors to Amorphous Materials”, *Inorg. Chem.*, **2004**, *43*, 4615-4625
24. Razeghi, M., Houlier, B., Yuste, M., “EPR Study of Mn²⁺ Around the Ferroelastic Transition Point of Pb₃(PO₃)₂”, *Sol. St. Comm.*, **1978**, *26*, 665-668

ToC Graphic:

